

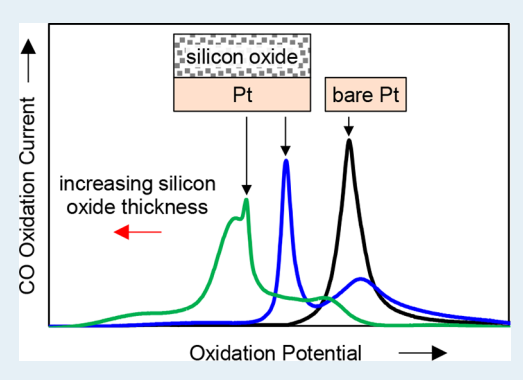
# Silicon Oxide-Encapsulated Platinum Thin Films as Highly Active Electrocatalysts for Carbon Monoxide and Methanol Oxidation

Jacob E. Robinson, <sup>†</sup> Natalie Y. Labrador, <sup>†</sup> Han Chen, B. Edward Sartor, and Daniel V. Esposito \*

Department of Chemical Engineering, Columbia Electrochemical Energy Center, Lenfest Center for Sustainable Energy, Columbia University in the City of New York, 500 W. 120th Street, New York, New York 10027, United States

Supporting Information

**ABSTRACT:** Direct alcohol fuel cells (DAFCs) have the potential to provide high power densities for transportation and portable applications. However, widespread use of DAFCs is greatly hindered by the lack of anode electrocatalysts that are inexpensive, stable, resistant to CO poisoning, and highly active toward alcohol oxidation. One promising approach to overcoming these challenges is to combine transition metal catalysts with oxide supports, such as  $SiO_2$ , which are known to enhance alcohol oxidation by promoting CO oxidation at oxidelmetal interfacial regions through the so-called bifunctional mechanism. Herein, we report on a membrane-coated electrocatalyst (MCEC) architecture for alcohol oxidation, in which a thin, permeable silicon oxide ( $SiO_x$ ) nanomembrane encapsulates a well-defined Pt thin film ( $SiO_x|Pt$ ). A key advantage of the MCEC design compared to oxide-supported nanoparticles is that the oxide encapsulation maximizes the



density of oxidelmetal interfacial sites between the  $SiO_x$  and Pt catalyst. A series of electroanalytical measurements indicates that the  $SiO_x$  overlayers provide proximal hydroxyls, in the form of silanol groups, which can enhance alcohol oxidation by interacting with adsorbed intermediates at  $SiO_x$ lPt interfaces. Thanks to these interactions, the  $SiO_x$ lPt electrocatalysts exhibit significantly enhanced CO oxidation activity and roughly a 2-fold increase in the maximum methanol oxidation current density compared to bare Pt. Overall, these demonstrations highlight the potential of using  $SiO_x$ -based MCECs for CO tolerant and highly active methanol oxidation electrocatalysts.

**KEYWORDS:** electrocatalysis, confined catalysis, carbon monoxide oxidation, methanol oxidation, membrane-coated electrocatalyst, bifunctional mechanism, overlayers, silicon dioxide

## 1. INTRODUCTION

Small alcohol fuels, such as methanol and ethanol, are attractive energy carriers for a sustainable energy future because of their high energy densities, ease of storage as liquids, and the ability to produce them electrochemically from carbon dioxide (CO<sub>2</sub>) and water (H<sub>2</sub>O) using electricity from renewable resources. 1-4 These alcohol fuels can be converted back into electricity for various applications using direct alcohol fuel cells (DAFCs), where alcohol oxidation at the anode is coupled with the oxygen reduction reaction (ORR) at the cathode. 5,6 Despite recent advances in the performance of DAFCs,<sup>5</sup> their power densities ( $\approx 0.01-10 \text{ W cm}^{-2}$ ) are still significantly lower than hydrogen fuel cells (HFCs), which typically achieve power densities of  $\approx 10-100 \text{ W cm}^{-2.7}$  Major reasons for the performance gap between DAFCs and HFCs are voltage losses that originate from (i) fuel crossover to the cathode and (ii) sluggish reaction kinetics associated with alcohol oxidation at the DAFC anode. 8,9 The state-of-the-art anode catalysts in acidic medium are based on nanoparticles of platinum (Pt) or Pt alloys that are supported on high surface area carbon (Pt/C). The performance of DAFC anodes can also suffer from degradation of the electrocatalyst and carbon support, which can lead to dissolution, detachment,

migration, and/or agglomeration of the catalytic nano-particles. 13-15

In order to reduce kinetic overpotential losses associated with the methanol oxidation reaction (MOR) and ethanol oxidation reaction (EOR), significant research efforts have been made to better understand the mechanisms that underlie these reactions. It is now well understood that the MOR and EOR are complex multistep reactions that require catalytic sites for alcohol adsorption and dehydrogenation, as well as sites that facilitate oxidation of carbonaceous intermediates to the desired end product, carbon dioxide (CO<sub>2</sub>).<sup>2,16-20</sup> Many studies have highlighted the importance of efficiently oxidizing carbon monoxide (CO), a commonly observed intermediate in alcohol oxidation that can "poison" active sites that bind CO too strongly. 5,21 Others have found that CO oxidation is more favorable when oxygen-containing coreactants such as adsorbed hydroxyl groups  $(OH_{ad})$  are located in close proximity to the adsorbed  $CO.^{22-24}$  The two most common methods to introduce oxygen-containing species near active

Received: September 8, 2018 Revised: October 19, 2018 Published: October 24, 2018



sites, and thereby improve CO tolerance, are (i) to alloy Ptbased catalysts with a second metal that has a higher affinity for oxygen (more oxophilic), such as ruthenium (Ru)<sup>25,26</sup> or tin (Sn), 27,28 and (ii) to support metal nanoparticles on metal oxide supports that contain hydroxyl groups. 28-36 The enhanced electrocatalytic activity of Pt electrocatalysts for the MOR and EOR by these two modifications is attributed to the so-called bifunctional mechanism whereby metallic Pt provides sites to initially adsorb and dehydrogenate the alcohol while the oxophilic material supplies oxygen-containing species that subsequently oxidize the adsorbed carbonaceous intermediates to CO<sub>2</sub>. 37 Alloying Pt with Ru or Sn has proven to be effective for alleviating CO poisoning issues, 25-28 but it does not address the issue of carbon support oxidation. As a result, oxide materials have attracted considerable attention as supports for alcohol oxidation electrocatalysts due to their: (i) higher corrosion resistance than carbon, (ii) abundance of hydroxyl groups to facilitate CO removal, and (iii) potential to suppress catalyst particle migration thanks to partial encapsulation and/or stronger bonding between the oxide material and the metal nanoparticles.<sup>38–41</sup> In particular, metal oxide supports, such as CeO<sub>2</sub>, <sup>42,43</sup> MgO, <sup>44</sup> WO<sub>3</sub>, <sup>45</sup> SnO<sub>2</sub>, <sup>28</sup> and TiO<sub>2</sub>, <sup>30–32</sup> have demonstrated enhanced activity toward alcohol oxidation when paired with Pt nanoparticles.

Motivated by prior studies on metal oxide supports for alcohol oxidation, the current paper investigates oxidelmetal electrocatalysts for methanol oxidation that are composites of silicon oxide ( $\mathrm{SiO}_x$ ) and Pt. Similar to many other oxides supports,  $\mathrm{SiO}_x$  contains hydroxyl groups, in the form of silanols ( $\mathrm{Si-OH}$ ),  $^{46-48}$  which have been shown to promote CO oxidation on Pt electrocatalysts. Additionally, silica ( $\mathrm{SiO}_2$ ) is known to have excellent chemical stability in acidic and neutral pHs.  $^{49}$  Many studies have demonstrated improved MOR activity and stability with  $\mathrm{SiO}_2$  supported Pt catalysts, with most suggesting that silanol groups suppress CO poisoning and thereby enhance MOR activity through the bifunctional mechanism.  $^{50-54}$  Pt/SiO<sub>2</sub> catalysts have also shown enhanced EOR activity compared to Pt/graphite.  $^{55}$ 

Despite the promising reports of high alcohol oxidation activity with Pt/oxide composite electrocatalysts, two common concerns are the lower surface areas and electrical conductivities of oxides such as silica compared to conventional carbon supports.<sup>54</sup> Consequently, studies that involve oxide supports typically require intricate modifications to improve their low electrical conductivity and surface area. To improve the electrical conductivity,  $TiO_2$  is commonly doped with Nb,  $^{56,57}$  C,  $^{58}$  or N.  $^{59}$  For  $SiO_2$  supports, unique architectures have been employed to increase conductivity and surface area such as incorporating Pt/silica into mesoporous conductive carbon supports<sup>60</sup> and functionalizing hollow SiO<sub>2</sub> spheres with amino acids to help anchor Pt onto SiO<sub>2</sub> and SiO<sub>2</sub> onto conductive supports.<sup>54</sup> Although these approaches can effectively improve CO tolerance, they often require complex, high temperature synthesis methods to produce the precise composition, structure, and loading. Moreover, methods that involve high temperature treatment could ultimately decrease the specific surface area of the support and catalyst.

In order to compensate for the low surface areas of oxide supports and minimize catalyst loading, researchers have also tried to minimize catalyst nanoparticle size, albeit at the expense of accelerated dissolution of the smaller nanoparticles. 61,62 If smaller (<5 nm) Pt nanoparticles could be

stabilized on oxide supports, Ting et al. suggested that they could better take advantage of the bifunctional mechanism compared to larger particles because a higher percentage of the Pt sites would be located in close proximity to the hydroxylcontaining oxide support. Extending this logic further, we hypothesize that the most active alcohol oxidation electrocatalysts are those that are designed to maximize the number of active sites for alcohol adsorption/dehydrogenation that are in close proximity to hydroxyl sites for CO oxidation.

Toward this end, we explore  $SiO_x|Pt$  alcohol oxidation electrocatalysts based on the membrane-coated electrocatalyst (MCEC) architecture,  $^{63}$  in which the active metal electrocatalyst (Pt) is encapsulated by an ultrathin (<10 nm thick) oxide layer that can exhibit membrane-like transport properties.  $^{64}$  The  $SiO_x$  overlayers used in this study are fabricated with a low-temperature ultraviolet ozone (UV ozone) photochemical synthesis procedure to deposit ultrathin (<10 nm), permeable silicon oxide nanomembranes over well-defined Pt thin film electrocatalysts ( $SiO_x|Pt$ ), as depicted schematically in Figure 1. The underlying motivations for

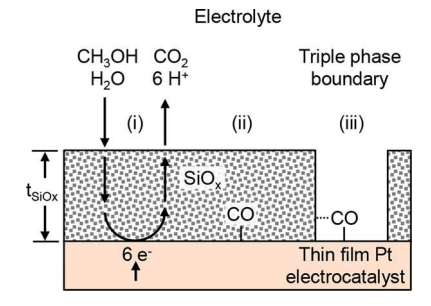


**Figure 1.** Schematic side view illustrating methanol oxidation at a planar Pt electrocatalyst encapsulated by an ultrathin, permeable  $\mathrm{SiO}_x$  overlayer with thickness  $t_{\mathrm{SiO}_x}$  that enables (i) diffusion of electroactive species to and from the electrocatalytic  $\mathrm{SiO}_x$ lPt buried interface. Also shown are adsorbed CO intermediates located at (ii) the buried interface and (iii) an opening in the  $\mathrm{SiO}_x$  film which can create a triple phase boundary site.

investigating these  $SiO_x$ lPt MCECs are their potential to (i) maximize interfacial contact between the Pt catalyst and hydroxyl-containing  $SiO_x$  overlayer, (ii) suppress corrosion of the metal nanoparticles and the underlying conductive support, and (iii) create unique active sites at the oxidelmetal buried interface through confinement effects. 65–67

MCEC-type architectures have been previously employed to stabilize nanoparticles or molecular catalysts in fuel cells<sup>68-76</sup> and photoelectrochemical cells. 77-79 Takenaka et al. demonstrated that silica coatings on Pt nanoparticle catalysts improved durability and minimized particle agglomeration and dissolution for the ORR but found that the same electrodes exhibited poor activity for the MOR and EOR compared to uncoated Pt/C nanoparticle catalysts. 73 The poor alcohol oxidation activity was attributed to suppressed transport of small polar alcohols across the hydrophobic silica used in that study. In contrast, we report herein on the use of hydrophilic SiO<sub>x</sub>|Pt MCECs that enhance alcohol oxidation. We have recently shown that SiO, overlayers, fabricated with the UV ozone method, are effective at suppressing Pt nanoparticle migration<sup>79</sup> and facilitating transport of protons (H<sup>+</sup>) and hydrogen molecules (H<sub>2</sub>) between the bulk electrolyte and SiO<sub>2</sub>|Pt buried interface.<sup>64</sup> In the current paper, we extend the use of these hydrophilic  $SiO_x$  overlayers,

deposited on planar Pt films, to study CO oxidation and MOR at SiO<sub>x</sub>lPt interfaces (Figure 1). These model thin film electrodes are an attractive platform for studying these reactions because they have very well-defined catalyst surface areas, avoid complexities/nonuniformities associated with nanoparticles, and allow for detailed characterization of the buried oxidelmetal interface. The thin film SiO<sub>x</sub>lPt electrodes in this study demonstrate that the MCEC design leverages the high density of reaction sites at SiO, IPt interfaces to readily oxidize intermediates and increase MOR activity compared to bare Pt electrodes. Furthermore, the impact of varied potential and pH conditions on Pt-OH<sub>ad</sub>, PtO<sub>x</sub>, and Si-OH formation are evaluated to elucidate the role of hydroxyl groups on Pt and SiO<sub>x</sub> during the MOR. Overall, this study shows that the SiO<sub>x</sub>-encapsulated Pt electrocatalysts can enhance methanol oxidation with minimal diffusion barrier to methanol transport to SiO, Pt interfaces.

## 2. EXPERIMENTAL METHODS

**2.1. Electrode Preparation.** A detailed description of the procedure for synthesizing Pt and SiO, IPt thin film electrodes can be found in our previous publication.<sup>64</sup> Briefly, a 4.5 nm thick Ti adhesion layer and 50 nm thick Pt film were sequentially deposited by electron-beam evaporation onto degeneratively doped Si(100) conductive substrates (p+Si, WRS materials). Next, a mixture of the trimethylsiloxy terminated polydimethylsiloxane (PDMS) precursor dissolved in toluene 80,81 (1.2 and 3.0 mg mL<sup>-1</sup> for SiO<sub>x</sub> films with final thicknesses of  $\approx 2$  and  $\approx 5$  nm, respectively) was spin coated onto the metal-coated samples for 2.5 min at 4000 rpm. After drying in a vacuum oven, the PDMS was converted into SiO, under UV light in air for 2 h within a UV ozone cleaning system (UVOCS, T10X10/OES). 80,82 Electrical contacts were made by soldering a Cu wire to the back side of the electrode substrate. Electrodes were then sealed with vinyl 3M Electroplating Tape 470, which possessed circular openings with an area of 0.246 cm<sup>2</sup> through which the electrode was exposed to the electrolyte. All current densities reported herein were normalized by the geometric area of this opening.

**2.2. Structural Characterization.** The thicknesses of the SiO<sub>x</sub> overlayers were measured using a Woollam alpha-SE ellipsometer. Raw ellipsometry data was fit with a Cauchy model, and a standard error in thickness was determined for all of the  $\approx$ 2 nm (sample size N=2) and  $\approx$ 5 nm (N=6) thick samples used in this study. The morphology of the SiO<sub>x</sub> thin films was analyzed with a Bruker Dimension Icon atomic force microscopy (AFM) using the identical imaging parameters previously reported.<sup>64</sup> X-ray photoelectron spectroscopy (XPS) characterization was performed with a Phi XPS instrument equipped with a monochromatic aluminum  $K\alpha$ X-ray source (15 kV, 20 mA) and operated with a pass energy of 23.5 eV and a charge neutralizer. The charge neutralizer was calibrated to give a C 1s peak center of 284.5 eV, after which the Si 2p, O 1s, and Pt 4f spectra were shifted by the same value. Overlayer composition and atomic ratios were determined on the basis of peak areas and tabulated atomic sensitivity factors (ASF<sub>i</sub>). 83 An ASF<sub>Si</sub> of 0.339 was used for Si to account for differences in density and attenuation lengths of metallic Si and SiO<sub>2</sub>.

**2.3. Electroanalytical Measurements.** A SP-200 Bio-Logic potentiostat was used for conducting all electroanalytical measurements. A carbon rod (Saturn Industries) counter electrode and a AglAgCl/sat. 3 M KCl reference electrode ( $E^{\circ}$ 

= 0.21 V vs NHE, Hach, E21M002) were used in a standard three electrode configuration. Cyclic voltammetry (CV) measurements used to determine the electrochemically active surface areas (ECSAs) from hydrogen underpotential deposition  $(H_{upd})$  signal were performed in deaerated 0.5 M sulfuric acid that was prepared from 18  $M\Omega$  deionized water and concentrated sulfuric acid (H<sub>2</sub>SO<sub>4</sub>, Fisher Scientific, ACS grade). The ECSAs were calculated as previously described<sup>64</sup> and are based on a conversion factor of 210  $\mu$ C  $H_{\rm upd}$  signal per cm<sup>-2</sup> Pt for polycrystalline Pt.<sup>84</sup> The reported  $H_{\rm upd}$ -derived ESCAs are average values determined from analysis of CV cycles 100-150. CO stripping voltammetry experiments were also performed in 0.5 M H<sub>2</sub>SO<sub>4</sub>. First, CO was adsorbed from a CO-saturated 0.5 M H<sub>2</sub>SO<sub>4</sub> electrolyte onto the electrode surface at +0.05 V vs RHE for 3 min. While the electrode was held at this potential, excess CO in solution was subsequently removed by purging the solution with N<sub>2</sub> gas for 20 min. Adsorbed CO was then stripped (oxidized) from the electrode surface by scanning the applied potential from 0.22 V to 0.0 V to 1.2 V vs RHE at 20 mV s<sup>-1</sup>. Upon reaching the positive scan vertex, the scan direction was reversed to complete the first CV cycle. A second CV cycle was subsequently recorded over the same potential range to verify that no CO remained adsorbed on the electrode after the first cycle. The moles of adsorbed CO initially present on the electrode surface were then calculated on the basis of the difference in the integrated charge recorded during the positive scan segments of the first and second CV cycles. Methanol oxidation experiments were performed in 0.5 M H<sub>2</sub>SO<sub>4</sub> with 0.5 M methanol (CH<sub>3</sub>OH, Fisher Chemical, ACS grade). CVs were performed for 100 cycles and typically reached a steady state by cycle 15. In examining the effect of the CV vertex on electrochemical activity, the upper vertex potential was increased from 0.8 to 1.2 V vs RHE in 100 mV increments. Each upper vertex was maintained for 15 cycles to allow the sample to reach a steady state. Following the last cycle with an upper vertex potential of 1.2 V vs RHE, the vertex was decreased back to 0.8 V vs RHE to evaluate any discrepancy from the beginning of cycling. Potassium hydroxide (KOH, Sigma-Aldrich, ACS reagent) was used to remove SiO, from Pt for control experiments, in which samples were exposed to SiO<sub>x</sub> synthesis conditions. KOH etching was performed in 20 wt % KOH with 3 v/v % isopropyl alcohol (C<sub>3</sub>H<sub>8</sub>OH, Fisher Chemical, ACS reagent) for 10 min at 75 °C. Experiments in neutral pH electrolytes were performed in a 0.1 M sodium phosphate buffer solution (Na<sub>2</sub>HPO<sub>4</sub>/NaH<sub>2</sub>PO<sub>4</sub>, Sigma-Aldrich, Reagent Plus).

## 3. RESULTS

**3.1. Characterization of SiO**<sub>x</sub> **Overlayer.** As-made SiO<sub>x</sub>l Pt and Pt thin films were first characterized by ellipsometry, AFM, and XPS to evaluate their composition and structure. The thicknesses of SiO<sub>x</sub> overlayers were determined by ellipsometry and found to be  $2.4 \pm 0.2$  and  $5.4 \pm 0.3$  nm. For simplicity, these samples are referred to herein as 2 nm SiO<sub>x</sub>lPt and 5 nm SiO<sub>x</sub>lPt. As-made samples were also characterized with AFM to view differences in the topology of SiO<sub>x</sub> overlayers and bare Pt films. All samples possessed uniform and smooth topologies that were characterized by root mean squared (rms) surface roughness values of 0.95, 0.55, and 0.41 nm for the bare Pt, 2 nm SiO<sub>x</sub>lPt, and 5 nm SiO<sub>x</sub>lPt electrodes, respectively (Figure S1). AFM images indicated that microscopic holes were not present on these SiO<sub>x</sub> overlayers. SiO<sub>x</sub>lPt electrodes were further characterized with

XPS (Figure S2), which showed that the  $SiO_x$  overlayers made by the UV ozone process were primarily comprised of silicon dioxide ( $SiO_2$ ), as evidenced by the Si 2p peak center located at 103.5 eV and relatively low concentration of carbon (C) ( $\approx$ 8 atomic % C). These results are consistent with previously reported XPS characterization of  $SiO_x$  layers synthesized using the UV ozone photochemical conversion process. <sup>80,82</sup>

The electrochemically active surface areas (ECSAs) of Pt and  $SiO_x$ |Pt electrodes were evaluated from the integrated  $H_{upd}$  signal recorded during CV cycling in deaerated 0.5 M  $H_2SO_4$ . The steady state voltammograms for the 0 nm (bare Pt), 2 nm, and 5 nm  $SiO_x$ |Pt samples are provided in Figure 2. All samples

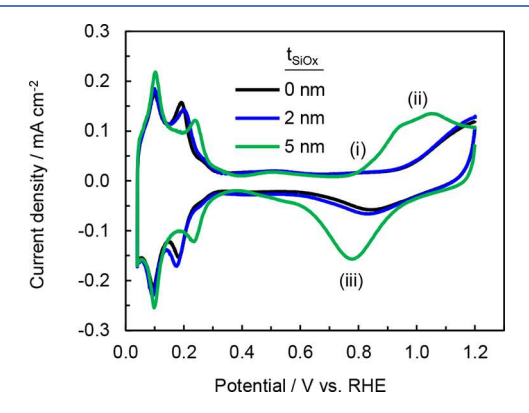


**Figure 2.** CV curves (30th cycle) recorded at 100 mV s<sup>-1</sup> in deaerated 0.5 M  $H_2SO_4$  for  $SiO_x$ |Pt electrodes containing:  $t_{SiO_x} = 0$  nm (black),  $t_{SiO_x} = 2$  nm (blue), and  $t_{SiO_x} = 5$  nm (green)  $SiO_x$  films.

exhibit H<sub>upd</sub> signal and Pt-oxide formation/reduction peaks that are characteristic of polycrystalline Pt electrodes in sulfuric acid. 85,86 Analysis of the integrated  $H_{\rm upd}$  signal of CV cycles 100–150 gives average ECSA values of  $1.011 \pm 0.002$ ,  $1.064 \pm$ 0.001, and  $1.22 \pm 0.001$  cm<sup>2</sup> Pt per cm<sup>2</sup> geometric area for the 0, 2, and 5 nm samples, respectively. Similar to other publications, <sup>64,73,87</sup> the fact that the ECSA does not decrease for SiO, IPt electrodes attests to the ability of protons to transport through the SiO<sub>x</sub> overlayer and confirms that the buried interface between the SiOx and Pt thin film is electrochemically active. Despite having a similar  $H_{\rm upd}$ determined ECSA to the bare Pt control, the CV curve for the 5 nm SiO<sub>x</sub>IPt sample shows some key differences from bare Pt. In addition to slight shifts in the  $H_{\rm upd}$  peak locations, Figure 2 reveals significant differences in the features at more positive potentials associated with (i) formation of adsorbed oxygen species such as O<sub>ad</sub> and OH<sub>ad</sub>, (ii) their subsequent oxidation to form Pt-oxides, and (iii) reduction of these species during the negative scan. Notably, the onset of Pt oxidation shifts to slightly less positive potentials with increasing SiO<sub>x</sub> thickness. Similar shifts in the Pt-OH/PtO<sub>r</sub> formation features have been observed for Pt electrodes coated with thin SiO2 overlayers made by atomic layer deposition.<sup>87</sup> One possible explanation for these observations is that the SiO<sub>x</sub> overlayer alters the adsorption of sulfate ions, which are known to suppress the onset of surface oxidation of noble metal electrodes due to competitive adsorption.<sup>86</sup> However, it is also possible that SiO<sub>x</sub> overlayers can alter Pt-OH/PtO<sub>x</sub> dynamics at the SiO<sub>x</sub>IPt buried interface as a result of structural changes in the Pt surface caused by the highly oxidizing UV ozone conversion process and/or changes to the

electrochemical double layer (EDL) structure and, hence, the local electric field.

**3.2. CO Stripping Voltammetry.** Carbon monoxide (CO) stripping voltammetry was performed on  $SiO_x|Pt$  and bare Pt to simultaneously measure their ECSA and evaluate their ability to oxidize CO. Figure 3 compares the CO

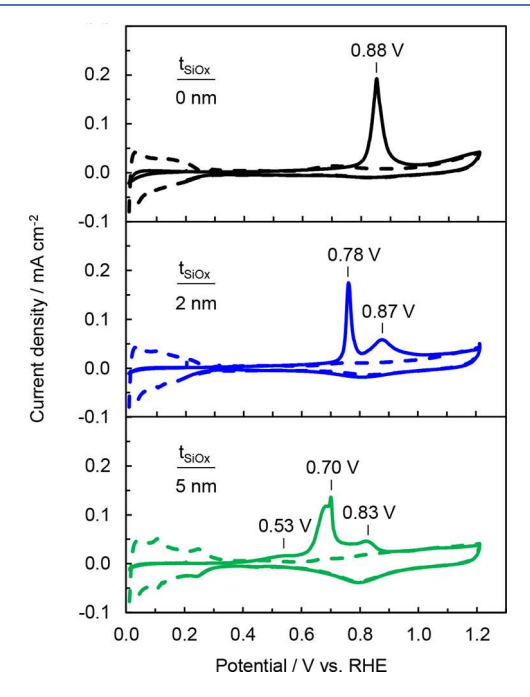


**Figure 3.** CO stripping voltammetry curves measured in 0.5 M  $\rm H_2SO_4$  at a scan rate of 20 mV s<sup>-1</sup> for Pt (black), 2 nm  $\rm SiO_x$ |Pt (blue), and 5 nm  $\rm SiO_x$ |Pt (green). Solid curves represent the first CV cycle that was carried out with CO adsorbed on the electrode surface, while dashed curves represent the second CV cycle that was performed after CO was stripped from the electrode surface during the first cycle.

stripping curves for 0 nm (bare Pt), 2 nm  $\mathrm{SiO_x}|\mathrm{Pt}$ , and 5 nm  $\mathrm{SiO_x}|\mathrm{Pt}$  electrodes. For all the electrodes, no  $H_{\mathrm{upd}}$  signal is observed in the first cycle (solid curves), indicating that almost all electroactive sites are occupied by adsorbed CO. As the potential is scanned to more positive potentials, distinct peaks associated with CO oxidation are observed for all electrodes. The second cycle (dashed curves) shows only  $H_{\mathrm{upd}}$  peaks and minor features associated with Pt—oxide formation and reduction, indicating that all of the adsorbed CO was fully oxidized and stripped from the electrode surface during the first cycle.

Although the integrated CO oxidation charge was similar for each sample, the location and number of peaks observed for each sample varied substantially. The peak centers of the main CO oxidation peak for the bare Pt and UV ozone treated bare Pt control samples (Figure S3) are located at 0.88 and 0.87 V vs RHE, respectively. These values are in good agreement with those reported in literature <sup>30,33</sup> and are consistent with the fact that Pt has a strong binding energy for CO. The 2 nm SiO<sub>x</sub>lPt and 5 nm SiO<sub>x</sub>lPt electrodes exhibit CO oxidation peaks that are shifted to more negative potentials, with peak centers located at 0.78 and 0.72 V vs RHE, respectively. Catalysts that require smaller overpotentials for CO oxidation are commonly described as "CO tolerant" because they require a smaller driving force to remove CO intermediates. <sup>20,35</sup> This enhanced ability to oxidize CO is often associated with the bifunctional

mechanism of methanol oxidation, especially for composite electrocatalysts in which Pt is combined with oxophilic materials. <sup>26,33,50</sup>

In addition to the primary CO oxidation peaks observed in Figure 3, smaller but distinct oxidation peaks are also observed at more positive potentials for the 2 and 5 nm SiO<sub>x</sub>lPt electrodes at 0.87 and 0.83 V vs RHE, respectively. These peak locations are similar to those observed for CO oxidation on bare Pt and may suggest that a small fraction of the Pt on the SiO, Pt electrodes still exhibit bare Pt-like behavior for CO oxidation. Another minor peak, shifted even more negative than the primary CO oxidation peaks for the SiO<sub>x</sub>lPt electrodes, is present at ≈0.53 V vs RHE. Importantly, the presence of this peak and the negative shift of the primary CO oxidation peaks strongly suggest that the reactive environments at the buried SiO<sub>x</sub>|Pt interface and/or SiO<sub>x</sub>|Pt|electrolyte triple phase boundary sites are very different from that at the electrolytelbare Pt interface. The negative shifts in the CO oxidation features of the SiOxIPt electrodes with respect to those of the bare Pt control samples indicate that the SiO<sub>x</sub>lPt is able to more easily oxidize adsorbed CO than Pt. Numerous studies on MOR electrocatalysts have connected a negative shift in the CO oxidation features to enhanced MOR activity, hypothesizing that the high activity is explained by lower CO binding energy and, therefore, lower susceptibility to CO poisoning.33,35,50

**3.3.** Cyclic Voltammetry in Methanol. The electrocatalytic activity of Pt and SiO<sub>x</sub>|Pt electrodes toward the electrooxidation of methanol was evaluated by performing 100 CV cycles in 0.5 M CH<sub>3</sub>OH in a deaerated 0.5 M H<sub>2</sub>SO<sub>4</sub> supporting electrolyte. Figure 4 compares the CVs for 0, 2, and 5 nm SiO<sub>x</sub>|Pt electrodes in 0.5 M methanol, for which the methanol oxidation half reaction is <sup>88</sup>

$$CH_3OH + H_2O \rightarrow CO_2 + 6H^+ + 6e^-$$
 (1)

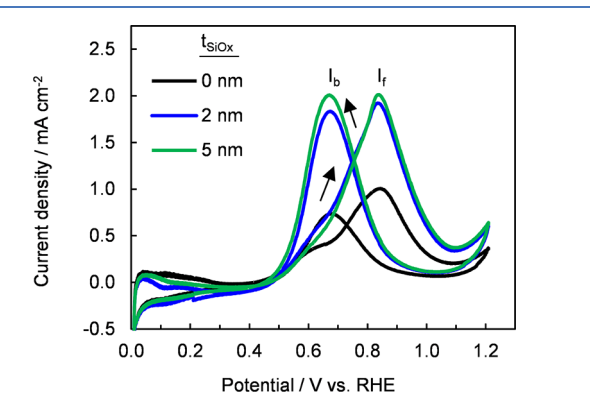


**Figure 4.** Cyclic voltammetry curves measured in 0.5 M CH<sub>3</sub>OH at a scan rate of 100 mV s<sup>-1</sup> for bare Pt (black), 2 nm  $SiO_x$ |Pt (blue), and 5 nm  $SiO_x$ |Pt (green) in deaerated 0.5 M H<sub>2</sub>SO<sub>4</sub> supporting electrolyte.

The MOR CV curves for all samples possess two primary oxidation peaks, which occur in the positive (forward) and negative (backward) scan directions and are centered at 0.84 and 0.65 V vs RHE, respectively. The magnitude of the current density in the forward direction,  $I_{\rm f}$ , is seen to be  $\approx 2$  times larger for the SiO<sub>x</sub>|Pt electrodes compared to the bare Pt control sample, despite having similar ECSAs based on the  $H_{\rm und}$  signal. The SiO<sub>x</sub>|Pt electrodes also exhibit significantly

higher current densities than bare Pt throughout 15 min chronoamperometry (CA) measurements at both +0.6 V vs RHE and +0.8 V vs RHE (Figure S4), confirming that their higher activity seen in CV measurements is not a transient phenomenon.

Another difference in the CV curves for the SiO<sub>x</sub>|Pt and bare Pt electrodes is the relative magnitude of  $I_f$  to the peak current density recorded during the backward scan, Ib. Recent studies have demonstrated that both of these peaks have the same chemical origin and can be primarily attributed to oxidation of methanol, as opposed to earlier studies suggesting that most of the current observed in negative scan originated from oxidation of residual carbon intermediates.<sup>89,90</sup> The hysteresis in the MOR peaks for Pt electrodes is now understood to arise from differences in Pt surface oxidation state during the positive and negative scan directions.<sup>89</sup> In the positive (forward) scan, methanol oxidation occurs on Pt before it is suppressed by the formation of a high coverage of Pthydroxides (Pt-OH<sub>ad</sub>) and/or Pt-oxides (PtO<sub>x</sub>) at more positive potentials. After the scan direction is reversed at the positive scan vertex, methanol oxidation gradually increases again as Pt-OH<sub>ad</sub> and PtO<sub>x</sub> species are reduced to free up metallic Pt sites that are known to be more active for methanol decomposition. By this means, the extent of Pt oxidation that occurs during the scan to positive potentials greatly impacts the peak MOR current density that occurs during the negative (backward) scan  $(I_b)$  as well as the ratio of the forward peak current  $(I_f)$  to  $I_h$ . Due to the important role of Pt-oxides, the ratio of MOR peak current densities  $(I_f/I_h)$  can be used as an indicator of the catalyst oxophilicity, which is described as the metallic (M) catalyst's susceptibility to form M-OH or MO<sub>x</sub> species.  $^{89,91}$  Electrocatalysts with large  $I_{\mathrm{f}}/I_{\mathrm{b}}$  are those with a high affinity for oxygen (oxophilic), while those with small  $I_f/I_b$ are less readily oxidized or are more easily reactivated by reducing the oxidized form back to the metallic state. 89,91 From the CV curves in Figure 4,  $I_f/I_h$  ratios of 1.32  $\pm$  0.02, 1.06  $\pm$ 0.01, and 1.00  $\pm$  0.02 are computed for the 0, 2, and 5 nm  $SiO_x$ lPt electrodes, respectively. The differences in  $I_f/I_h$ between samples suggest that there are differences in the oxophilicity between the SiO<sub>x</sub>lPt and Pt electrodes. The relationship between the  $I_f/I_b$  ratios, catalyst oxophilicity, and Pt-OH<sub>ad</sub> and PtO<sub>r</sub> coverage are discussed further below.

Because the CV curves in Figure 4 were recorded in a sulfuric acid supporting electrolyte, it must be pointed out that sulfate/bisulfate anions are known to suppress methanol oxidation activity of Pt electrocatalysts due to their ability to compete with OH adsorption on the electrocatalyst surface. 92-94 Because of this effect, peak methanol oxidation current densities recorded for Pt electrocatalysts in sulfuric acid are always lower than those recorded in perchloric acid, for which perchlorate anions adsorb much more weakly to the Pt surface than (bi)sulfate anions. 95 Given that previous studies have shown SiO<sub>x</sub> overlayers capable of serving as selective transport barriers, <sup>64,96</sup> it is plausible that the enhanced methanol oxidation activity of SiO<sub>x</sub>lPt electrodes could arise from the ability of SiO<sub>x</sub> overlayers to block (bi)sulfate ions from reaching the active sites at the SiO<sub>x</sub>|Pt buried interface. This hypothesis was tested by performing methanol oxidation CVs with bare Pt and 5 nm SiO<sub>x</sub>|Pt electrodes in 0.5 M H<sub>2</sub>SO<sub>4</sub> and 0.5 M HClO<sub>4</sub> (Figure S5). Two identical samples were tested for each sample type to avoid sample history effects. Figure S5 shows that the peak methanol oxidation current densities in the perchloric acid supporting electrolyte increased

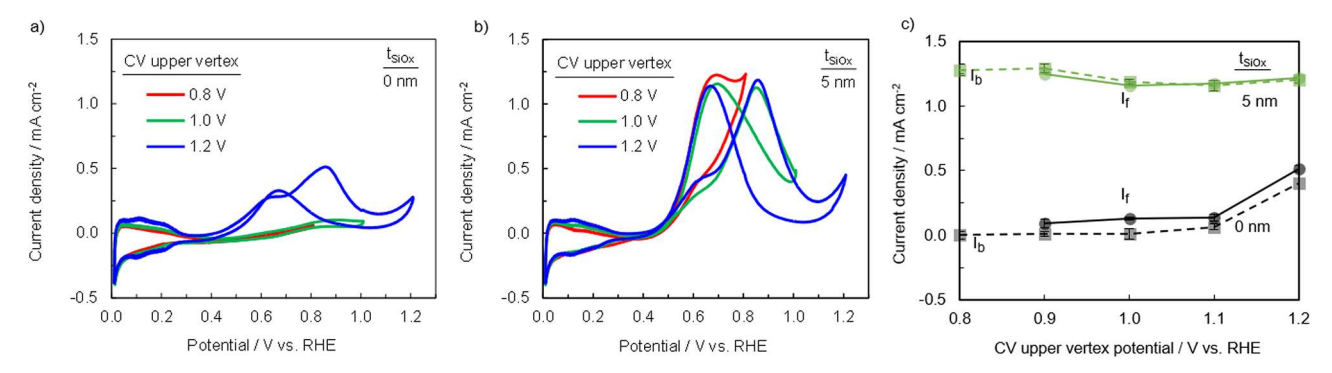


**Figure 5.** Methanol oxidation CVs (steady state cycle 15) with different upper scan vertices for (a)  $t_{SiO_x} = 0$  nm and (b)  $t_{SiO_x} = 5$  nm  $SiO_x|Pt$  MCEC. (c) Peak MOR current densities recorded during the forward ( $I_f$ ) and backward ( $I_b$ ) scan segments as a function of upper vertex potential. CVs were performed in 0.5 M H<sub>2</sub>SO<sub>4</sub> containing 0.5 M CH<sub>3</sub>OH and measured at 100 mV s<sup>-1</sup>.

by  $\approx 65\%$  compared to those recorded in sulfuric acid for both bare Pt and SiO<sub>x</sub>lPt electrodes. The observation of similar "anion effects" for both bare Pt and SiO<sub>x</sub>lPt electrodes indicates that (i) sulfate anions are still capable of reaching the buried SiO<sub>x</sub>lPt interface and (ii) the SiO<sub>x</sub> overlayer must be impacting the methanol oxidation activity in other ways besides blocking sulfate ions. The ability of sulfate ions to permeate into the SiO<sub>x</sub> overlayers can be understood by the need to maintain electroneutrality within the SiO<sub>x</sub> overlayer and is consistent with our previous study that looked at SiO<sub>x</sub>lPt thin film electrodes for the hydrogen evolution reaction in 0.5 M H<sub>2</sub>SO<sub>4</sub>. Regardless of the extent that SiO<sub>x</sub> suppresses the adsorption of (bi)sulfate anions, Figures 4 and S5 demonstrate that SiO<sub>x</sub>lPt electrodes possess superior MOR activity compared to bare Pt.

3.4. Role of Pt-OH<sub>ad</sub> and PtO<sub>x</sub> on Methanol Oxidation Activity. Several studies have shown that the extent of Pt oxidation can influence CO oxidation and MOR activity. While the formation of Pt-oxides  $(PtO_x, x = 1 \text{ or } 2)^{97}$ has a prohibitive effect on MOR activity, 89,91,98 the presence of intermediate coverages of Pt-hydroxides, Pt-OH<sub>ad</sub>, is believed to assist in CO removal to allow continual MOR.89 To investigate the role of Pt-oxides on the MOR for bare Pt and SiO<sub>x</sub>|Pt electrodes, MOR CVs were carried out where the upper vertex potential was incrementally increased. Upper scan vertices ranging between 0.8 and 1.2 V were chosen to transition between conditions where Pt oxidation would be avoided or favored, on the basis of the Pt-OH<sub>ad</sub> and PtO<sub>x</sub> features observed in the control CV curves performed in 0.5 M H<sub>2</sub>SO<sub>4</sub> without methanol (Figure 2). Figure 5 shows MOR CVs for bare Pt and 5 nm SiO<sub>x</sub>lPt electrodes with upper vertices of 0.8, 1.0, and 1.2 V vs RHE. The effects of the positive vertex potential on the forward and backward scan peak currents are summarized in Figure 5c, with the complete set of CV curves provided in Figure S6. Figure 5a shows that the bare Pt electrode exhibits very low MOR activity for CVs with positive vertex potentials less than 1.1 V vs RHE but that a sudden jump in MOR activity is achieved once the scan vertex is more positive than 1.1 V vs RHE. In contrast, Figure 5b shows the SiO<sub>x</sub>IPt electrode achieves high MOR activity regardless of upper vertex potential. Interestingly, when the potential vertex was changed back to 0.8 V vs RHE (Figure S4), the bare Pt showed an increased MOR activity similar to the CV performed at 1.2 V vs RHE, while the MOR activity of the SiO<sub>x</sub>|Pt remained high for all CV scans. These results demonstrate the formation of Pt-OH<sub>ad</sub> and PtO<sub>x</sub>, specifically

at more oxidizing potentials, has a strong effect on initiating MOR activity for bare Pt but has essentially no effect for SiO<sub>x</sub>l Pt. For bare Pt, the upper potential vertex that leads to an increase in MOR activity approximately coincides with the onset potential for Pt oxidation, as observed in Figure 2. This result is consistent with many previous studies on Pt-based MOR electrocatalysts that have shown the importance of having some Pt-OH<sub>ad</sub> species in order to facilitate removal of adsorbed CO intermediates. Meanwhile, for SiO<sub>x</sub>lPt, the lack of dependency of the MOR peak currents on the upper scan rate suggests that the formation of Pt-OH<sub>ad</sub> may not be necessary to accelerate methanol oxidation.

**3.5. Electrocatalyst Stability.** Figure 6 contains the 1st, 10th, 50th, and 100th CV cycles for bare Pt and 5 nm SiO<sub>x</sub>IPt electrodes during MOR. The MOR peak currents for bare Pt

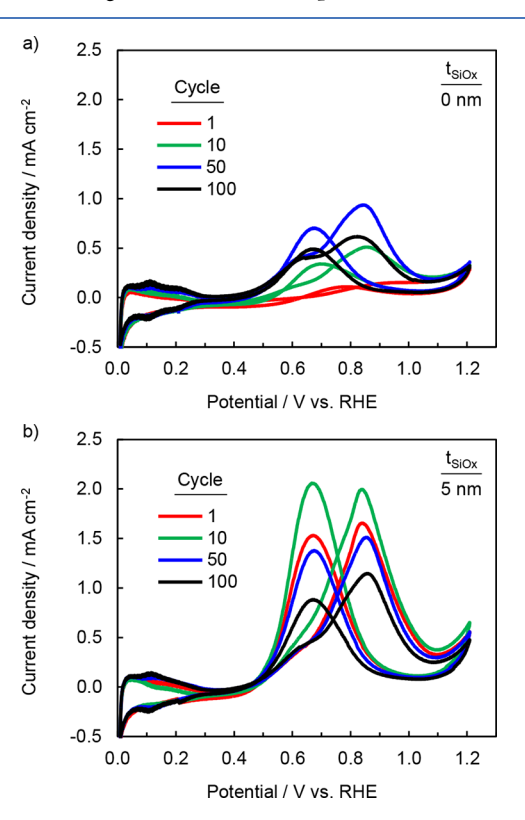


**Figure 6.** 1st (red), 10th (green), 50th (blue), and 100th (black) CV cycles for (a) bare Pt and (b) 5 nm  $SiO_x$ IPt in 0.5 M  $H_2SO_4$  containing 0.5 M  $CH_3OH$  and measured at 100 mV  $s^{-1}$ .

rapidly increase for the first 10 cycles before reaching maximum values between 10 and 50 cycles. Some decline in MOR peak current is observed toward the end of CV cycling, possibly due to the gradual depletion of methanol from the bulk electrolyte caused by slow evaporation of methanol into the headspace. The transient nature of the MOR peak current densities during CV cycling was very different for the SiO<sub>x</sub>lPt electrodes, which show very high initial MOR peak current densities that gradually decrease with cycle number (Figure 6b). Despite the decreasing MOR current densities, the peak current densities of the SiO, IPt electrodes still exceeded those of the bare Pt electrode at the end of CV cycling. Control MOR experiments on KOH etched bare Pt and 5 nm SiO<sub>x</sub>|Pt, in which no SiO<sub>x</sub> remained after the KOH etch, show no difference in MOR activity, confirming that the presence of the SiO<sub>x</sub> film is necessary for enhanced MOR current densities, relative to bare Pt (Figure S7). This result suggests that (some) SiO<sub>x</sub> must still be present on the electrode at the end of CV cycling to maintain higher currents than Pt. In addition to methanol depletion, the gradual decrease in SiO<sub>x</sub>lPt activity may be related to changes in the SiO<sub>x</sub> structure, as evidenced by AFM and XPS analysis of MCEC samples after CV cycling (Figures S8 and S9) that show possible SiO<sub>x</sub> delamination and/or SiO, "island" formation. Although the SiO, Pt electrocatalysts appear to be susceptible to degradation during extended cycling, the repeated oxidation/reduction of Pt/PtO. during CV cycling is likely to cause stress at the SiO<sub>x</sub>lPt interface. The repeated restructuring of the SiO<sub>x</sub>lPt interface may lead to gradual delamination of the SiO<sub>x</sub> overlayer, especially for thin film electrodes where the SiO<sub>x</sub> is only attached to Pt. In fuel cell-relevant nanoparticle/support systems, SiO<sub>x</sub> will primarily be adhered to an inert support material such as carbon for which delamination should be less of an issue in the absence of significant electrochemistry at the SiO<sub>x</sub>lsupport buried interface.

## 4. DISCUSSION

The results in Figures 3 and 4 demonstrate that deposition of  $SiO_x$  onto Pt thin films significantly enhances their catalytic activity toward methanol oxidation compared to bare Pt. Similar observations have been made in prior studies of silicon oxide supported Pt nanoparticle electrocatalysts, with the improved performance most commonly attributed to hydroxylfacilitated removal of CO intermediates through the aforementioned bifunctional mechanism. S0-S4,100 In order to design catalysts that are more CO tolerant, it is important to understand the source of the hydroxyl groups that are responsible for aiding in the removal of adsorbed CO intermediates on Pt (Pt-CO<sub>ad</sub>). As expressed in eqs 2 and 3, CO oxidation may be achieved through reactions with silanol groups attached to  $SiO_x$  ( $SiO_x$ -OH) or hydroxyls on Pt (Pt-OH)<sup>8,12,61,101</sup>

$$Pt-CO_{ad} + SiO_x - OH \rightarrow Pt + SiO_2 + CO_2 + H^+ + e^-$$
(2)

$$Pt-CO_{ad} + Pt-OH_{ad} \rightarrow 2Pt + CO_2 + H^+ + e^-$$
 (3)

where, in both cases, hydroxyls must be regenerated through an additional oxidation step.

$$SiO_x + H_2O \leftrightarrow SiO_x - OH_{ad} + H^+ + e^-$$
 (4)

$$Pt + H_2O \leftrightarrow Pt - OH_{ad} + H^+ + e^-$$
 (5)

Prior studies on SiO<sub>2</sub>-supported MOR catalysts have suggested that silanol groups may enhance MOR activity by accelerating CO oxidation as a part of the bifunctional (2-site) mechanism. 50-54,100 In this study, Figure 2 shows that the presence of SiO<sub>x</sub> overlayers can also affect Pt oxophilicity and, likely, the coverage of Pt-OH<sub>ad</sub> at a given applied potential. If CO and methanol oxidation occur at the buried interface of MCECs, it is expected that the presence of the SiO<sub>x</sub> may also indirectly influence reaction energetics at the buried interface through confinement (steric) effects, varying concentrations of reactants and spectator ions near active sites, and alteration of electric fields caused by disruption of the electrochemical double layer. A density functional theory study investigating confined catalysis determined the adsorption energy of CO on Pt was lowered due to the presence of a graphene overlayer which destabilized the CO<sub>ad</sub> molecule.<sup>67</sup> That study indicates that the confined environments at the buried interface between graphene and Pt can greatly alter the interactions and energetics between molecules and the active electrocatalyst. Similarly, the SiO<sub>x</sub> overlayers studied in this work may directly and/or indirectly influence alcohol oxidation kinetics. If the mechanisms by which the SiO<sub>x</sub> overlayers influence electrocatalysis of SiO, IPt electrodes can be better understood, that information can be used to guide the design of MCECs with even better CO tolerance and alcohol oxidation activity.

The CO stripping results in Figure 3 showed that the presence of 5 nm of SiO<sub>x</sub> on Pt shifts CO oxidation features by 100 and 200 mV relative to those for the 2 nm SiO<sub>x</sub>lPt and bare Pt electrodes, respectively. Despite the very positive oxidation potential required to form hydroxyls on bare Pt (>0.85 V vs RHE), 86,102 SiO<sub>x</sub>IPt is still able to achieve high MOR currents at moderate oxidation potentials (Figure 5b), which suggests hydroxyls are readily available at lower oxidation potentials for the bifunctional mechanism. The silanol groups on SiO<sub>x</sub> that are present in acidic environments<sup>46–48</sup> may serve as an abundant source of hydroxyls that are in close proximity to Pt-CO<sub>ad</sub> at the SiO<sub>x</sub>|Pt interface. We also hypothesize that the SiO<sub>x</sub> may change the Pt oxophilicity to make Pt-OH formation more energetically favorable at lower overpotentials, as suggested by the negative shift in the onset potential of Pt oxidation with increasing SiO<sub>x</sub> thickness. This trend in the Pt oxidation onset potential may be related to the negative shift in the CO oxidation onset potentials for the 2 and 5 nm SiO<sub>x</sub>|Pt samples (0.70 to 0.60 V vs RHE, respectively). However, it must also be noted that the onset for CO oxidation for the 5 nm SiO<sub>x</sub>|Pt occurs at 200-300 mV more negative than the onset of Pt-oxidation features, meaning that it is unlikely that Pt-OH alone can explain the enhanced CO oxidation activity at more negative than 0.8 V vs RHE.

Hydroxyl species formed on Pt surfaces can enhance the MOR by promoting the bifunctional mechanism, as suggested by the initiation of MOR activity only after Pt-oxide (Pt-OH<sub>ad</sub> and PtO<sub>x</sub>) formation (Figure 5a). Additional insights into the role of Pt-OH species can be obtained by analyzing the ratio of the peak current densities during methanol oxidation CVs ( $I_f/I_b$ ), as mentioned in Section 3.3. In studies on PtRu MOR electrocatalysts, a high  $I_f/I_b$  ratio greater than 1 is commonly associated with a catalyst that is oxophilic. A study focused on the origin of the low  $I_b$  concluded that the propensity for PtRu catalysts to more easily form oxygenated species during CV excursions to the positive scan vertex inhibits the MOR during the negative (backward) scan segment because the high OH<sub>ad</sub> and oxide coverage blocks

catalytic sites and thereby lowers  $I_{\rm b}$ . In other words, hydroxyls are necessary for the promotion of MOR, but excessive OH<sub>ad</sub> and/or oxide coverage on catalytic sites hinders further MOR due to the low abundance of metallic active sites. As a result, electrocatalysts that are more oxophilic tend to achieve high MOR activity in the positive (forward) scan,  $I_{tt}$ but lower MOR activity in the negative (backward) scan, Ib. This is why PtRu catalysts often have high  $I_f/I_h$ , especially compared to Pt. In contrast, SiO<sub>x</sub>IPt electrodes showed higher  $I_f$  and lower  $I_f/I_b$  than Pt in Figure 3 ( $I_f/I_b$  of 1.0 and 1.4, respectively). When the interpretation of the role of PtRu oxophilicity on MOR kinetics is extended to SiO<sub>x</sub>lPt electrocatalysts, the low  $I_f/I_b$  for SiO<sub>x</sub>lPt electrodes suggests these electrodes are less oxophilic than bare Pt. However, this statement seems to contradict the observations of more facile Pt-OH<sub>ad</sub>/PtO<sub>x</sub> formation for 5 nm SiO<sub>x</sub>|Pt in the CV curves in the 0.5 M H<sub>2</sub>SO<sub>4</sub> supporting electrolyte (Figure 2).

The different relationships between metal oxophilicity and MOR  $I_f/I_b$  peak ratios for SiO<sub>x</sub>|Pt electrocatalysts compared to PtRu electrocatalysts suggests that metal oxophilicity plays different roles in promoting MOR in these two types of electrocatalysts. Despite the higher oxophilicity, the high  $I_{\rm h}$ suggests that the SiO, IPt electrodes have a relatively moderate coverage of Pt-OH<sub>ad</sub> species during the backward scan that is conducive to higher MOR currents. Furthermore, the onset of  $I_{\rm b}$  has been shown to coincide with the reduction of Pt-OH<sub>ad</sub> and PtO<sub>x</sub>. Onsistent with these observations, this study on SiO<sub>x</sub>|Pt electrocatalysts suggests that oxophilic electrocatalysts may still exhibit high  $I_f$  and  $I_b$  so long as the kinetics of Pt-OH and PtO<sub>x</sub> reduction are fast enough to reactivate enough active sites for methanol decomposition during the backward scan. In other words, the  $I_f/I_b$  ratio correlates strongly with the ability of the metallic catalyst to regenerate hydroxyl species and/or metallic Pt sites, which can be referred to as a reactivation efficiency. Following this logic, the SiO<sub>x</sub>|Pt catalysts are oxophilic but also have a relatively high reactivation efficiency compared to bare Pt.

We hypothesize that the high oxophilicity and reactivation efficiency of the SiO<sub>x</sub>|Pt catalysts is due to hydroxyls from Si-OH that are not actually adsorbed onto the Pt surface but only share a proximity. Such proximal hydroxyls would not block Pt sites from methanol decomposition but instead would still be available to facilitate oxidation of CO intermediates through the bifunctional mechanism. Furthermore, proximal hydroxyls provided by Si-OH would allow for all of the Pt sites to be utilized for methanol decomposition, as opposed to conventional Pt electrocatalysts, where some fraction of the Pt surface must be occupied by Pt-OH<sub>ad</sub> (or Ru-OH<sub>ad</sub> in the case of PtRu alloy). This difference in available catalytic Pt sites may help explain the 2-fold increase in methanol oxidation current of SiO, Pt compared to Pt (Figure 4). Accordingly, the bifunctional mechanism is expected to proceed predominantly through silanol-mediated CO removal (eq 2) rather than CO oxidation by Pt-OH<sub>ad</sub> (eq 3). Therefore, the change in Pt oxophilicity observed for 5 nm SiO<sub>x</sub>lPt (Figure 2) may be a secondary effect of SiO<sub>x</sub> encapsulation that does not play a key role in determining MOR activity.

To better understand the role of  $SiO_x$  overlayers in facilitating the electrocatalytic properties of the  $SiO_x$ |Pt thin films, CO and methanol oxidation experiments were performed in a pH 7 sodium phosphate buffer solution in which silanol groups may become deprotonated. Silica is known to have two different types of silanol groups, each with

a different p $K_a$ .  $^{46-48,103}$  Silanol groups form when the solution pH is below the p $K_a$  of Si–OH (p $K_{a1} \approx 4$  and p $K_{a2} \approx 9$ ).  $^{46,47}$  Figure 7a shows CO stripping CVs for the bare Pt and 5 nm

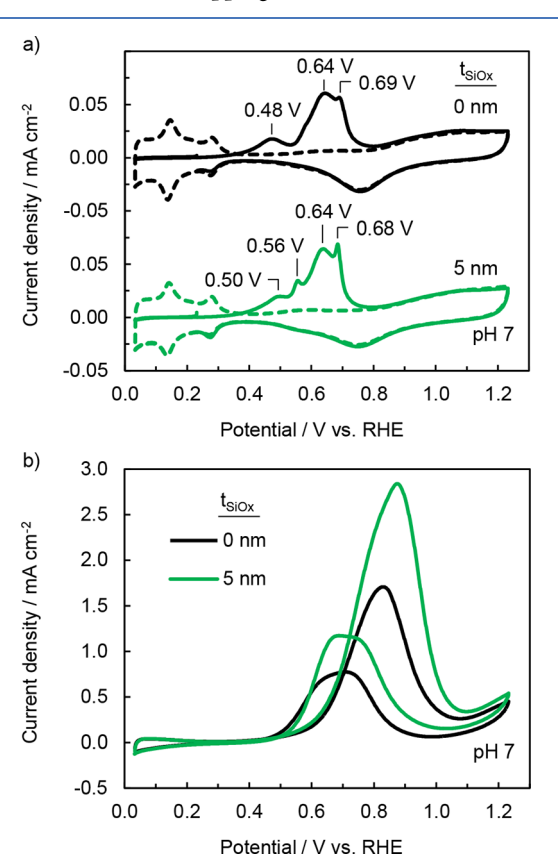


**Figure 7.** (a) CO stripping and (b) methanol oxidation CVs (cycle 30) in pH neutral electrolyte, 0.1 M sodium phosphate (buffered), with 0.5 M methanol for (b), for bare Pt (black) and 5 nm  $SiO_x$ lPt (green) electrodes at a scan rate of 100 mV s<sup>-1</sup>.

 $SiO_x$ |Pt at pH 7, for which the low-p $K_a$  silanol groups should be deprotonated. Both electrodes exhibit multiple CO oxidation peaks with similar onset potentials (0.40 and 0.44 V vs RHE) that are shifted more negative than in acidic media (Figure 3). These features and differences between acidic and neutral pH are consistent with CO oxidation on multifaceted Pt in alkaline electrolytes. 104,105 Importantly, the CO stripping curves are nearly identical for the SiOxIPt and Pt electrodes. If SiO<sub>x</sub>lPt was more active for CO oxidation than bare Pt in neutral pH, we would expect to observe a higher fraction of CO oxidation charge (i.e., a larger peak) at lower overpotentials. 105,106 In Figure 7a, the extent of CO oxidation at lower overpotentials (<0.6 V vs RHE) is nearly equivalent for both the SiO<sub>x</sub>IPt and Pt electrodes, indicating that the CO oxidation activity is similar for both electrocatalysts. This finding is consistent with the hypothesis that silanol groups on the SiO<sub>x</sub> overlayer boost CO oxidation activity, although differences in the structure of adsorbed CO layers in acidic and pH neutral environments may also be important factors in explaining why the CO oxidation curves converge.

Despite showing nearly identical CO stripping behavior as bare Pt in the pH neutral electrolyte, the  $SiO_x$ |Pt electrode still displayed significantly larger methanol oxidation activity in CV measurements conducted in the same pH = 7 supporting electrolyte (Figure 7b). It should also be noted that the ratio of

peak MOR currents,  $I_f/I_b$ , increased for both electrodes compared to those seen in the acidic electrolyte, from 1.4 to 2.3 for bare Pt and 1.0 to 2.5 for 5 nm SiO<sub>x</sub>|Pt, consistent with observations of methanol oxidation in more alkaline media.  $^{107-109}$  The observed increase in  $I_{\rm f}/I_{\rm b}$  for  ${\rm SiO_x lPt}$  in neutral pH to a value that is similar to that for silanol-free bare Pt lends further support to the hypothesis that proximal silanols were responsible for the low  $I_f/I_h$  ratio for SiO<sub>x</sub>lPt in the acidic electrolyte. However, it does not explain why the supposedly silanol-stripped SiO<sub>x</sub>IPt electrodes still maintain a higher MOR activity than bare Pt at neutral pH. One explanation is local acidification at the buried SiO, IPt interface, which might arise from suppressed diffusion of protons back to the bulk electrolyte that were generated by the MOR (eq 1). Local acidification could help to keep silanol groups protonated even though the pH of the bulk electrolyte is above the silanol  $pK_{a1}$ . It is also possible that silanol groups associated with p $K_{a2}$  of SiO<sub>2</sub>, which are still protonated at pH = 7, are still able to participate in the MOR at more positive potentials, even though they do not appear to influence CO oxidation at less positive potentials (Figure 7a). However, the enhanced MOR current for SiO<sub>x</sub>IPt compared to bare Pt at the neutral pH might also result from the aforementioned "indirect" mechanisms by which the SiO<sub>x</sub> overlayer can alter reaction energetics without directly being involved as an active site. Although this study was not able to fully deconvolute the influences of the SiOx overlayer on methanol oxidation, we expect that in situ spectroscopies and computational tools will be of great value in future studies aimed at a deeper molecular understanding of electrocatalysis at buried interfaces.

## 5. CONCLUSIONS

The planar MCEC architecture investigated in this work provided a well-defined platform to investigate the unique electrocatalytic properties of the oxide-encapsulated metal electrocatalyst. In this study, we examined the effect of 2-5 nm thick SiO<sub>x</sub> overlayers on Pt catalyst films for alcohol oxidation in acidic media. These SiO, MCECs demonstrated lower CO oxidation onset potentials during CO stripping voltammetry than Pt in an acidic supporting electrolyte. The increased CO tolerance is likely due to the ability of silanol groups on SiO<sub>x</sub> to promote oxidation of adsorbed CO on Pt. Furthermore, the SiO<sub>x</sub>lPt MCECs exhibit a 2-fold increase in the maximum peak current densities for alcohol oxidation compared to Pt. The enhanced performance toward alcohol oxidation, in acidic electrolyte, is largely attributed to the interactions between proximal hydroxyls from silanol groups and adsorbed intermediates on Pt. These interfacial regions are maximized with the MCEC design, such that an abundance of hydroxyl groups is readily provided at SiO<sub>x</sub>|Pt interfaces where they can accelerate alcohol oxidation by the bifunctional mechanism. Varied CV vertex potential and pH measurements suggest that silanol groups, which are present at all relevant potentials in acidic pH, are active participants in CO and methanol oxidation. Although the MOR activity of SiO<sub>x</sub>|Pt electrodes decreases during long-time cycling, this study demonstrates the MCEC design is a promising approach for CO tolerant and highly active alcohol oxidation electrocatalysts.

#### ASSOCIATED CONTENT

## Supporting Information

The Supporting Information is available free of charge on the ACS Publications website at DOI: 10.1021/acscatal.8b03626.

AFM and XPS characterization of  $SiO_x$  films, CO stripping on UV ozone treated Pt, methanol oxidation chronoamperometry, CV in methanol and perchloric acid, CV behavior for varied CV upper vertex potentials, methanol oxidation on etched electrodes, and AFM and XPS characterization of  $SiO_x$ IPt electrodes postmethanol CV measurements (PDF)

#### AUTHOR INFORMATION

## **Corresponding Author**

\*E-mail: de2300@columbia.edu. Phone: 212-854-2648.

#### ORCID ®

Jacob E. Robinson: 0000-0003-1865-3803 Natalie Y. Labrador: 0000-0003-2203-6584

Han Chen: 0000-0002-8262-4196

B. Edward Sartor: 0000-0001-6661-8645 Daniel V. Esposito: 0000-0002-0550-801X

#### **Author Contributions**

<sup>†</sup>J.E.R. and N.Y.L. contributed equally.

#### Notes

Any opinions, findings, and conclusions or recommendations expressed in this material are those of the author(s) and do not necessarily reflect the views of the National Science Foundation.

The authors declare no competing financial interest.

#### ACKNOWLEDGMENTS

The authors would like to acknowledge Xiangye Liu for helpful discussions and suggestions and the Columbia Nano Initiative (CNI) staff for assistance with deposition and characterization tools. D.V.E., J.E.R., and N.Y.L. acknowledge financial support from Columbia University start-up funds, Société de Chimie Industrielle (2017 Seifi Ghasemi/Air Products Scholarship), and the National Science Foundation (NSF) (CBET-1752340).

### REFERENCES

- (1) Moura, A.; Fajín, J.; Mandado, M.; Cordeiro, M. Ruthenium—Platinum Catalysts and Direct Methanol Fuel Cells (DMFC): A Review of Theoretical and Experimental Breakthroughs. *Catalysts* **2017**, *7*, 47.
- (2) Antolini, E. Electrocatalysis of Direct Methanol Fuel Cells: From Fundamentals to Applications; Liu, H., Zhang, J., Eds.; Wiley-VCH: Weinheim, Germany, 2009.
- (3) Léger, J.-M.; Rousseau, S.; Coutanceau, C.; Hahn, F.; Lamy, C. How Bimetallic Electrocatalysts Does Work for Reactions Involved in Fuel Cells? *Electrochim. Acta* **2005**, *50*, 5118–5125.
- (4) Kamarudin, M. Z. F.; Kamarudin, S. K.; Masdar, M. S.; Daud, W. R. W. Review: Direct Ethanol Fuel Cells. *Int. J. Hydrogen Energy* **2013**, 38, 9438–9453.
- (5) Chen, Y.; Bellini, M.; Bevilacqua, M.; Fornasiero, P.; Lavacchi, A.; Miller, H. A.; Wang, L.; Vizza, F. Direct Alcohol Fuel Cells: Toward the Power Densities of Hydrogen-Fed Proton Exchange Membrane Fuel Cells. *ChemSusChem* **2015**, *8*, 524–533.
- (6) Badwal, S. P. S.; Giddey, S.; Kulkarni, A.; Goel, J.; Basu, S. Direct Ethanol Fuel Cells for Transport and Stationary Applications A Comprehensive Review. *Appl. Energy* **2015**, *145*, 80—103.
- (7) Coutanceau, C.; Baranton, S. Electrochemical Conversion of Alcohols for Hydrogen Production: A Short Overview. *Wiley Interdiscip. Rev. Energy Environ.* **2016**, 5, 388–400.
- (8) Li, Q.; He, R.; Gao, J.-A.; Jensen, J. O.; Bjerrum, N. J. The CO Poisoning Effect in PEMFCs Operational at Temperatures up to 200°C. *J. Electrochem. Soc.* **2003**, *150*, A1599.

(9) Camara, G. A.; Ticianelli, E. A.; Mukerjee, S.; Lee, S. J.; McBreen, J. The CO Poisoning Mechanism of the Hydrogen Oxidation Reaction in Proton Exchange Membrane Fuel Cells. *J. Electrochem. Soc.* **2002**, *149*, A748.

- (10) McCabe, R. W.; McCready, D. F. Kinetics and Reaction Pathways of Methanol Oxidation on Platinum. *J. Phys. Chem.* **1986**, 90, 1428–1435.
- (11) Miller, A. V.; Kaichev, V. V.; Prosvirin, I. P.; Bukhtiyarov, V. I. Mechanistic Study of Methanol Decomposition and Oxidation on Pt(111). *J. Phys. Chem. C* **2013**, *117*, 8189–8197.
- (12) Rednyk, A.; Johánek, V.; Khalakhan, I.; Dubau, M.; Vorokhta, M.; Matolín, V. Methanol Oxidation on Sputter-Coated Platinum Oxide Catalysts. *Int. J. Hydrogen Energy* **2016**, *41*, 265–275.
- (13) He, Q.; Joy, D. C.; Keffer, D. J. Impact of Oxidation on Nanoparticle Adhesion to Carbon Substrates. *RSC Adv.* **2013**, *3*, 15792.
- (14) Dam, V. A. T.; de Bruijn, F. A. The Stability of PEMFC Electrodes. J. Electrochem. Soc. 2007, 154, B494.
- (15) Li, L.; Hu, L.; Li, J.; Wei, Z. Enhanced Stability of Pt Nanoparticle Electrocatalysts for Fuel Cells. *Nano Res.* **2015**, *8*, 418–440.
- (16) Iwasita, T. Handbook of Fuel Cells, Vol. 2.; Gasteiger, H. A., Kocha, S. S., Sompali, B., Wagner, F. T., Eds.; John Wiley & Sons, Ltd: London, 2010.
- (17) Iwasita, T. Electrocatalysis of Methanol Oxidation. *Electrochim. Acta* **2002**, 47, 3663–3674.
- (18) Nassr, A. B. A. A.; Sinev, I.; Pohl, M.-M.; Grünert, W.; Bron, M. Rapid Microwave-Assisted Polyol Reduction for the Preparation of Highly Active PtNi/CNT Electrocatalysts for Methanol Oxidation. *ACS Catal.* **2014**, *4*, 2449–2462.
- (19) Wasmus, S.; Küver, A. Methanol Oxidation and Direct Methanol Fuel Cells: A Selective Review. *J. Electroanal. Chem.* **1999**, *461*, 14–31.
- (20) Léger, J. M. Mechanistic Aspects of Methanol Oxidation on Platinum-Based Electrocatalysts. *J. Appl. Electrochem.* **2001**, 31, 767–771.
- (21) Tong, Y. J.; Kim, H. S.; Babu, P. K.; Waszczuk, P.; Wieckowski, A.; Oldfield, E. An NMR Investigation of CO Tolerance in a Pt/Ru Fuel Cell Catalyst. *J. Am. Chem. Soc.* **2002**, *124*, 468–473.
- (22) Zhang, K.; Yang, W.; Ma, C.; Wang, Y.; Sun, C.; Chen, Y.; Duchesne, P.; Zhou, J.; Wang, J.; Hu, Y.; Banis, M. N.; Zhang, P.; Li, F.; Li, J.; Chen, L. A Highly Active, Stable and Synergistic Pt Nanoparticles/Mo2C Nanotube Catalyst for Methanol Electro-Oxidation. NPG Asia Mater. 2015, 7, e153.
- (23) Scofield, M. E.; Koenigsmann, C.; Bobb-Semple, D.; Tao, J.; Tong, X.; Wang, L.; Lewis, C. S.; Vukmirovic, M. B.; Zhu, Y.; Adzic, R. R.; Wong, S. S. Correlating the Chemical Composition and Size of Various Metal Oxide Substrates with the Catalytic Activity and Stability of As-Deposited Pt Nanoparticles for the Methanol Oxidation Reaction. *Catal. Sci. Technol.* **2016**, *6*, 2435–2450.
- (24) Du, P.; Wu, P.; Cai, C. Mechanistic Insight into the Facet-Dependent Adsorption of Methanol on a Pt 3 Ni Nanocatalyst. *J. Phys. Chem. C* 2015, *119*, 18352–18363.
- (25) Liu, Z.; Ling, X. Y.; Su, X.; Lee, J. Y. Carbon-Supported Pt and PtRu Nanoparticles as Catalysts for a Direct Methanol Fuel Cell. *J. Phys. Chem. B* **2004**, *108*, 8234–8240.
- (26) Selvaraj, V.; Alagar, M. Pt and Pt-Ru Nanoparticles Decorated Polypyrrole/Multiwalled Carbon Nanotubes and Their Catalytic Activity towards Methanol Oxidation. *Electrochem. Commun.* **2007**, 9, 1145–1153.
- (27) Antolini, E.; Gonzalez, E. R. Effect of Synthesis Method and Structural Characteristics of Pt−Sn Fuel Cell Catalysts on the Electro-Oxidation of CH3OH and CH3CH2OH in Acid Medium☆. *Catal. Today* **2011**, *160*, 28−38.
- (28) Merati, Z.; Basiri Parsa, J. Enhancement of the Catalytic Activity of Pt Nanoparticles toward Methanol Electro-Oxidation Using Doped-SnO 2 Supporting Materials. *Appl. Surf. Sci.* **2018**, 435, 535–542.

- (29) Sharma, S.; Pollet, B. G. Support Materials for PEMFC and DMFC Electrocatalysts—A Review. *J. Power Sources* **2012**, 208, 96–119.
- (30) Qin, Y.-H.; Li, Y.; Lv, R.-L.; Wang, T.-L.; Wang, W.-G.; Wang, C.-W. Enhanced Methanol Oxidation Activity and Stability of Pt Particles Anchored on Carbon-Doped TiO2 Nanocoating Support. *J. Power Sources* **2015**, 278, 639–644.
- (31) Xing, L.; Jia, J.; Wang, Y.; Zhang, B.; Dong, S. Pt Modified TiO2 Nanotubes Electrode: Preparation and Electrocatalytic Application for Methanol Oxidation. *Int. J. Hydrogen Energy* **2010**, 35, 12169–12173.
- (32) Wu, X.; Zhuang, W.; Lu, L.; Li, L.; Zhu, J.; Mu, L.; Li, W.; Zhu, Y.; Lu, X. Excellent Performance of Pt-C/TiO2for Methanol Oxidation: Contribution of Mesopores and Partially Coated Carbon. *Appl. Surf. Sci.* **2017**, *426*, 890–896.
- (33) Zhuang, Y.; Ding, W.; Liu, Y.; Mou, Z.; Sun, J.; Guan, M. Reduced Nanostructured Titanium Oxide Coating as an Electrocatalyst Support for Methanol Oxidation. *J. Mater. Sci.* **2015**, *50*, 3875–3882.
- (34) Su, N.; Hu, X.; Zhang, J.; Huang, H.; Cheng, J.; Yu, J.; Ge, C. Plasma-Induced Synthesis of Pt Nanoparticles Supported on TiO2 Nanotubes for Enhanced Methanol Electro-Oxidation. *Appl. Surf. Sci.* **2017**, 399, 403–410.
- (35) Cui, G.; Shen, P. K.; Meng, H.; Zhao, J.; Wu, G. Tungsten Carbide as Supports for Pt Electrocatalysts with Improved CO Tolerance in Methanol Oxidation. *J. Power Sources* **2011**, *196*, 6125–6130
- (36) Ranga Rao, G.; Justin, P.; Meher, S. K. Metal Oxide Promoted Electrocatalysts for Methanol Oxidation. *Catal. Surv. Asia* **2011**, *15*, 221–229.
- (37) Watanabe, M.; Motoo, S. Electrocatalysis by Ad-Atoms. J. Electroanal. Chem. Interfacial Electrochem. 1975, 60, 267–273.
- (38) Liu, S.; Yu, W.; Chen, C.; Lo, A.; Hwang, B.; Chien, S.-H.; Liu, S.-B. Fabrication and Characterization of Well-Dispersed and Highly Stable PtRu Nanoparticles on Carbon Mesoporous Material for Applications in Direct Methanol Fuel Cell. *Chem. Mater.* **2008**, *20*, 1622–1628.
- (39) Kumar, A.; Ramani, V. Strong Metal—Support Interactions Enhance the Activity and Durability of Platinum Supported on Tantalum-Modified Titanium Dioxide Electrocatalysts. *ACS Catal.* **2014**, *4*, 1516—1525.
- (40) Pan, C.-J.; Tsai, M.-C.; Su, W.-N.; Rick, J.; Akalework, N. G.; Agegnehu, A. K.; Cheng, S.-Y.; Hwang, B.-J. Tuning/Exploiting Strong Metal-Support Interaction (SMSI) in Heterogeneous Catalysis. J. Taiwan Inst. Chem. Eng. 2017, 74, 154–186.
- (41) Kulesza, P. J.; Pieta, I. S.; Rutkowska, I. A.; Wadas, A.; Marks, D.; Klak, K.; Stobinski, L.; Cox, J. A. Electrocatalytic Oxidation of Small Organic Molecules in Acid Medium: Enhancement of Activity of Noble Metal Nanoparticles and Their Alloys by Supporting or Modifying Them with Metal Oxides. *Electrochim. Acta* 2013, 110, 474–483.
- (42) Xu, C.; Shen, P. K. Novel Pt/CeO2/C Catalysts for Electrooxidation of Alcohols in Alkaline Media. *Chem. Commun.* **2004**, *19*, 2238.
- (43) Xu, C.; Shen, P. K. Electrochamical Oxidation of Ethanol on Pt-CeO2/C Catalysts. *J. Power Sources* **2005**, *142*, 27–29.
- (44) Xu, C.; Shen, P. K.; Ji, X.; Zeng, R.; Liu, Y. Enhanced Activity for Ethanol Electrooxidation on Pt-MgO/C Catalysts. *Electrochem. Commun.* **2005**, *7*, 1305–1308.
- (45) Jayaraman, S.; Jaramillo, T. F.; Baeck, S.-H.; McFarland, E. W. Synthesis and Characterization of Pt–WO 3 as Methanol Oxidation Catalysts for Fuel Cells. *J. Phys. Chem. B* **2005**, *109*, 22958–22966.
- (46) Azam, M. S.; Weeraman, C. N.; Gibbs-Davis, J. M. Specific Cation Effects on the Bimodal Acid—Base Behavior of the Silica/Water Interface. *J. Phys. Chem. Lett.* **2012**, *3*, 1269–1274.
- (47) Ong, S.; Zhao, X.; Eisenthal, K. B. Polarization of Water Molecules at a Charged Interface: Second Harmonic Studies of the Silica/Water Interface. *Chem. Phys. Lett.* **1992**, *191*, 327–335.

(48) Leung, K.; Nielsen, I. M. B.; Criscenti, L. J. Elucidating the Bimodal Acid—Base Behavior of the Water—Silica Interface from First Principles. *J. Am. Chem. Soc.* **2009**, *131*, 18358—18365.

- (49) Pourbaix, M. Atlas of Electrochemical Equilibiria in Aqueous Solutions; Pergamon Press: Oxford; New York, 1974.
- (50) Tiwari, J. N.; Pan, F.-M.; Tiwari, R. N.; Nandi, S. K. Facile Synthesis of Continuous Pt Island Networks and Their Electrochemical Properties for Methanol Electrooxidation. *Chem. Commun.* **2008**, *48*, 6516.
- (51) Permyakova, A. A.; Han, B.; Jensen, J. O.; Bjerrum, N. J.; Shao-Horn, Y. Pt—Si Bifunctional Surfaces for CO and Methanol Electro-Oxidation. *J. Phys. Chem. C* **2015**, *119*, 8023–8031.
- (52) Tiwari, J. N.; Pan, F.-M.; Chen, T.-M.; Tiwari, R. N.; Lin, K.-L. Electrocatalytic Activity of Pt Nanoparticles Electrodeposited on Amorphous Carbon-Coated Silicon Nanocones. *J. Power Sources* **2010**. *195*, 729–735.
- (53) Vu, T. H. T.; Tran, T. T. T.; Le, H. N. T.; Tran, L. T.; Nguyen, P. H. T.; Nguyen, H. T.; Bui, N. Q. Solvothermal Synthesis of Pt-SiO2/Graphene Nanocomposites as Efficient Electrocatalyst for Methanol Oxidation. *Electrochim. Acta* **2015**, *161*, 335–342.
- (54) Melvin, A. A.; Joshi, V. S.; Poudyal, D. C.; Khushalani, D.; Haram, S. K. Electrocatalyst on Insulating Support?: Hollow Silica Spheres Loaded with Pt Nanoparticles for Methanol Oxidation. ACS Appl. Mater. Interfaces 2015, 7, 6590–6595.
- (\$5) Liu, B.; Chen, J. H.; Zhong, X. X.; Cui, K. Z.; Zhou, H. H.; Kuang, Y. F. Preparation and Electrocatalytic Properties of Pt–SiO2 Nanocatalysts for Ethanol Electrooxidation. *J. Colloid Interface Sci.* **2007**, 307, 139–144.
- (56) Huang, S.-Y.; Ganesan, P.; Popov, B. N. Electrocatalytic Activity and Stability of Niobium-Doped Titanium Oxide Supported Platinum Catalyst for Polymer Electrolyte Membrane Fuel Cells. *Appl. Catal., B* **2011**, *102*, 71–77.
- (57) Rigdon, W. A.; Huang, X. Carbon Monoxide Tolerant Platinum Electrocatalysts on Niobium Doped Titania and Carbon Nanotube Composite Supports. *J. Power Sources* **2014**, *272*, 845–859.
- (58) Hahn, R.; Schmidt-Stein, F.; Salonen, J.; Thiemann, S.; Song, Y.; Kunze, J.; Lehto, V.-P.; Schmuki, P. Semimetallic TiO 2 Nanotubes. *Angew. Chem., Int. Ed.* **2009**, *48*, 7236–7239.
- (59) Zhu, J.; Žhao, X.; Xiao, M.; Liang, L.; Liu, C.; Liao, J.; Xing, W. The Construction of Nitrogen-Doped Graphitized Carbon—TiO2 Composite to Improve the Electrocatalyst for Methanol Oxidation. *Carbon* **2014**, 72, 114–124.
- (60) Tang, H.; Jiang, S. P. Self-Assembled Pt/Mesoporous Silica—Carbon Electrocatalysts for Elevated-Temperature Polymer Electrolyte Membrane Fuel Cells. *J. Phys. Chem. C* **2008**, *112*, 19748–19755.
- (61) Ting, C.-C.; Liu, C.-H.; Tai, C.-Y.; Hsu, S.-C.; Chao, C.-S.; Pan, F.-M. The Size Effect of Titania-Supported Pt Nanoparticles on the Electrocatalytic Activity towards Methanol Oxidation Reaction Primarily via the Bifunctional Mechanism. *J. Power Sources* **2015**, 280, 166–172.
- (62) Ting, C.-C.; Chao, C.-H.; Tsai, C. Y.; Cheng, I.-K.; Pan, F.-M. Electrocatalytic Performance of Pt Nanoparticles Sputter-Deposited on Indium Tin Oxide toward Methanol Oxidation Reaction: The Particle Size Effect. *Appl. Surf. Sci.* **2017**, *416*, 365–370.
- (63) Esposito, D. V. Membrane-Coated Electrocatalysts—An Alternative Approach To Achieving Stable and Tunable Electrocatalysis. ACS Catal. 2018, 8, 457–465.
- (64) Labrador, N. Y.; Songcuan, E. L.; De Silva, C.; Chen, H.; Kurdziel, S. J.; Ramachandran, R. K.; Detavernier, C.; Esposito, D. V. Hydrogen Evolution at the Buried Interface between Pt Thin Films and Silicon Oxide Nanomembranes. ACS Catal. 2018, 8, 1767–1778.
- (65) Doyle, A. D.; Montoya, J. H.; Vojvodic, A. Improving Oxygen Electrochemistry through Nanoscopic Confinement. *ChemCatChem* **2015**, *7*, 738–742.
- (66) Fu, Y.; Rudnev, A. V.; Wiberg, G. K. H.; Arenz, M. Single Graphene Layer on Pt(111) Creates Confined Electrochemical Environment via Selective Ion Transport. *Angew. Chem., Int. Ed.* **2017**, *56*, 12883–12887.

- (67) Li, H.; Xiao, J.; Fu, Q.; Bao, X. Confined Catalysis under Two-Dimensional Materials. *Proc. Natl. Acad. Sci. U. S. A.* **2017**, *114*, 5930–5934.
- (68) Takenaka, S.; Matsumori, H.; Arike, T.; Matsune, H.; Kishida, M. Preparation of Carbon Nanotube-Supported Pt Metal Particles Covered with Silica Layers and Their Application to Electrocatalysts for PEMFC. *Top. Catal.* **2009**, *52*, 731–738.
- (69) Matsumori, H.; Takenaka, S.; Matsune, H.; Kishida, M. Preparation of Carbon Nanotube-Supported Pt Catalysts Covered with Silica Layers; Application to Cathode Catalysts for PEFC. *Appl. Catal.*, A 2010, 373, 176–185.
- (70) Takenaka, S.; Susuki, N.; Miyamoto, H.; Tanabe, E.; Matsune, H.; Kishida, M. Highly Durable Pd Metal Catalysts for the Oxygen Reduction Reaction in Fuel Cells; Coverage of Pd Metal with Silica. *Chem. Commun.* **2010**, *46*, 8950–8952.
- (71) Takenaka, S.; Susuki, N.; Miyamoto, H.; Tanabe, E.; Matsune, H.; Kishida, M. Highly Durable Carbon Nanotube-Supported Pd Catalysts Covered with Silica Layers for the Oxygen Reduction Reaction. J. Catal. 2011, 279, 381–388.
- (72) Takenaka, S.; Matsumori, H.; Matsune, H.; Kishida, M. Highly Durable Pt Cathode Catalysts for Polymer Electrolyte Fuel Cells; Coverage of Carbon Black-Supported Pt Catalysts with Silica Layers. *Appl. Catal.*. A 2011, 409–410, 248–256.
- (73) Takenaka, S.; Miyamoto, H.; Utsunomiya, Y.; Matsune, H.; Kishida, M. Catalytic Activity of Highly Durable Pt/CNT Catalysts Covered with Hydrophobic Silica Layers for the Oxygen Reduction Reaction in PEFCs. J. Phys. Chem. C 2014, 118, 774–783.
- (74) Takenaka, S.; Miyazaki, T.; Matsune, H.; Kishida, M. Highly Active and Durable Silica-Coated Pt Cathode Catalysts for Polymer Electrolyte Fuel Cells: Control of Micropore Structures in Silica Layers. Catal. Sci. Technol. 2015, 5, 1133–1142.
- (75) Yaowarat, W.; Li, O. L.; Saito, N. Highly Durable Silica Coated Pt/Cs with Different Surfactant Types for Proton Exchange Membrane Fuel Cell Applications. *RSC Adv.* **2015**, *5*, 44258–44262.
- (76) Yaowarat, W.; Li, O. L. H.; Saito, N. Highly Durable Silica-Coated Pt/Carbon Nanotubes for Proton-Exchange Membrane Fuel Cells Application. *Jpn. J. Appl. Phys.* **2016**, *55*, 01AE23.
- (77) Gu, J.; Yan, Y.; Young, J. L.; Steirer, K. X.; Neale, N. R.; Turner, J. A. Water Reduction by a P-GaInP2 Photoelectrode Stabilized by an Amorphous TiO2 Coating and a Molecular Cobalt Catalyst. *Nat. Mater.* **2016**, *15*, 456–460.
- (78) Garcia-Esparza, A. T.; Shinagawa, T.; Ould-Chikh, S.; Qureshi, M.; Peng, X.; Wei, N.; Anjum, D. H.; Clo, A.; Weng, T.-C.; Nordlund, D.; Sokaras, D.; Kubota, J.; Domen, K.; Takanabe, K. An Oxygen-Insensitive Hydrogen Evolution Catalyst Coated by a Molybdenum-Based Layer for Overall Water Splitting. *Angew. Chem., Int. Ed.* **2017**, *56*, *5780*–*5784*.
- (79) Labrador, N. Y.; Li, X.; Liu, Y.; Tan, H.; Wang, R.; Koberstein, J. T.; Moffat, T. P.; Esposito, D. V. Enhanced Performance of Si MIS Photocathodes Containing Oxide-Coated Nanoparticle Electrocatalysts. *Nano Lett.* **2016**, *16*, 6452–6459.
- (80) Mirley, C.; Koberstein, J. A Room Temperature Method for the Preparation of Ultrathin SiOx Films from Langmuir-Blodgett Layers. *Langmuir* **1995**, *11*, 1049.
- (81) Phely-Bobin, T. S.; Muisener, R. J.; Koberstein, J. T.; Papadimitrakopoulos, F. Site-Specific Self-Assembly of Si/SiOx Nanoparticles on Micropatterned Poly(Dimethylsiloxane) Thin Films. Synth. Met. 2001, 116, 439–443.
- (82) Ouyang, M.; Yuan, C.; Muisener, R. J.; Boulares, a.; Koberstein, J. T. Conversion of Some Siloxane Polymers to Silicon Oxide by UV/ Ozone Photochemical Processes. *Chem. Mater.* **2000**, *12*, 1591–1596.
- (83) Moulder, J. F.; Stickle, W. F.; Sobol, P. E.; Bomben, K. D. *Handbook of X-Ray Photoelectron Spectroscopy*; Chastain, J., King, R. C. J., Eds.; Physical Electronics, Inc.: Eden Prairie, MN, 1995.
- (84) Biegler, T.; Rand, D. A. J.; Woods, R. Limiting Oxygen Coverage on Platinized Platinum; Relevance to Determination of Real Platinum Area by Hydrogen Adsorption. *J. Electroanal. Chem. Interfacial Electrochem.* 1971, 29, 269–277.

(85) Angerstein-Kozlowska, H.; Conway, B. E.; Sharp, W. B. A. The Real Condition of Electrochemically Oxidized Platinum Surfaces. Part I. Resolution of Component Processes. *J. Electroanal. Chem. Interfacial Electrochem.* **1973**, 43, 9–36.

- (86) Conway, B. E. E. Electrochemical Oxide Film Formation at Noble Metals as a Surface-Chemical Process. *Prog. Surf. Sci.* **1995**, 49, 331–452.
- (87) Yuan, G.; Agiral, A.; Pellet, N.; Kim, W.; Frei, H. Inorganic Core-shell Assemblies for Closing the Artificial Photosynthetic Cycle. *Faraday Discuss.* **2014**, *176*, 233–249.
- (88) Lamy, C.; Guenot, B.; Cretin, M.; Pourcelly, G. (Invited) A Kinetics Analysis of Methanol Oxidation under Electrolysis/Fuel Cell Working Conditions. *ECS Trans.* **2015**, *66*, 1–12.
- (89) Chung, D. Y.; Lee, K.-J.; Sung, Y.-E. Methanol Electro-Oxidation on the Pt Surface: Revisiting the Cyclic Voltammetry Interpretation. *J. Phys. Chem. C* **2016**, *120*, 9028–9035.
- (90) Hofstead-Duffy, A. M.; Chen, D.-J.; Sun, S.-G.; Tong, Y. J. Origin of the Current Peak of Negative Scan in the Cyclic Voltammetry of Methanol Electro-Oxidation on Pt-Based Electro-catalysts: A Revisit to the Current Ratio Criterion. *J. Mater. Chem.* **2012**, *22*, 5205.
- (91) Zhao, Y.; Li, X.; Schechter, J. M.; Yang, Y. Revisiting the Oxidation Peak in the Cathodic Scan of the Cyclic Voltammogram of Alcohol Oxidation on Noble Metal Electrodes. *RSC Adv.* **2016**, *6*, 5384–5390.
- (92) Markovic, N. M.; Lucas, C. A.; Rodes, A.; Stamenkovic, V.; Ross, P. N. Surface Electrochemistry of CO on Pt(111): Anion Effects. Surf. Sci. 2002, 499, L149–L158.
- (93) Grozovski, V.; Climent, V.; Herrero, E.; Feliu, J. M. The Role of the Surface Structure in the Oxidation Mechanism of Methanol. *J. Electroanal. Chem.* **2011**, *662*, 43–51.
- (94) Housmans, T. H. M.; Wonders, A. H.; Koper, M. T. M. Structure Sensitivity of Methanol Electrooxidation Pathways on Platinum: An on-Line Electrochemical Mass Spectrometry Study. *J. Phys. Chem. B* **2006**, *110*, 10021–10031.
- (95) Wang, H.; Baltruschat, H. DEMS Study on Methanol Oxidation at Poly- and Monocrystalline Platinum Electrodes: The Effect of Anion, Temperature, Surface Structure, Ru Adatom, and Potential. *J. Phys. Chem. C* **2007**, *111*, 7038–7048.
- (96) Yuan, G.; Agiral, A.; Pellet, N.; Kim, W.; Frei, H. Inorganic Core Shell Assemblies for Closing the Artificial Photosynthetic Cycle. *Faraday Discuss.* **2014**, *176*, 233–249.
- (97) Redmond, E. L.; Setzler, B. P.; Alamgir, F. M.; Fuller, T. F. Elucidating the Oxide Growth Mechanism on Platinum at the Cathode in PEM Fuel Cells. *Phys. Chem. Chem. Phys.* **2014**, *16*, 5301.
- (98) Eickes, C.; Piela, P.; Davey, J.; Zelenay, P. Recoverable Cathode Performance Loss in Direct Methanol Fuel Cells. *J. Electrochem. Soc.* **2006**, *1*53, A171.
- (99) Tripković, A. V.; Popović, K. Đ.; Momčilović, J. D.; Dražić, D. M. Kinetic and Mechanistic Study of Methanol Oxidation on a Pt(110) Surface in Alkaline Media. *Electrochim. Acta* 1998, 44, 1135–1145.
- (100) Nam, K.; Lim, S.; Kim, S. K.; Yoon, S. H.; Jung, D. H. Application of Silica as a Catalyst Support at High Concentrations of Methanol for Direct Methanol Fuel Cells. *Int. J. Hydrogen Energy* **2012**, *37*, 4619–4626.
- (101) Markovic, N. Surface Science Studies of Model Fuel Cell Electrocatalysts. Surf. Sci. Rep. 2002, 45, 117–229.
- (102) Jerkiewicz, G.; Vatankhah, G.; Lessard, J.; Soriaga, M. P.; Park, Y.-S. Surface-Oxide Growth at Platinum Electrodes in Aqueous H2SO4. *Electrochim. Acta* **2004**, *49*, 1451–1459.
- (103) Pfeiffer-Laplaud, M.; Costa, D.; Tielens, F.; Gaigeot, M.-P.; Sulpizi, M. Bimodal Acidity at the Amorphous Silica/Water Interface. *J. Phys. Chem. C* **2015**, *119*, 27354–27362.
- (104) Spendelow, J. S.; Goodpaster, J. D.; Kenis, P. J. A.; Wieckowski, A. Mechanism of CO Oxidation on Pt(111) in Alkaline Media. *J. Phys. Chem. B* **2006**, *110*, 9545–9555.
- (105) Spendelow, J. S.; Lu, G. Q.; Kenis, P. J. A.; Wieckowski, A. Electrooxidation of Adsorbed CO on Pt(111) and Pt(111)/Ru in

Alkaline Media and Comparison with Results from Acidic Media. *J. Electroanal. Chem.* **2004**, *568*, 215–224.

- (106) Wang, Y.; Wang, G.; Li, G.; Huang, B.; Pan, J.; Liu, Q.; Han, J.; Xiao, L.; Lu, J.; Zhuang, L. Pt—Ru Catalyzed Hydrogen Oxidation in Alkaline Media: Oxophilic Effect or Electronic Effect? *Energy Environ. Sci.* **2015**, *8*, 177—181.
- (107) Tripković, A.; Popović, K.; Grgur, B.; Blizanac, B.; Ross, P.; Marković, N. Methanol Electrooxidation on Supported Pt and PtRu Catalysts in Acid and Alkaline Solutions. *Electrochim. Acta* **2002**, *47*, 3707–3714.
- (108) Cohen, J. L.; Volpe, D. J.; Abruña, H. D. Electrochemical Determination of Activation Energies for Methanol Oxidation on Polycrystalline Platinum in Acidic and Alkaline Electrolytes. *Phys. Chem. Chem. Phys.* **2007**, *9*, 49–77.
- (109) Spendelow, J. S.; Goodpaster, J. D.; Kenis, P. J. A.; Wieckowski, A. Methanol Dehydrogenation and Oxidation on Pt(111) in Alkaline Solutions. *Langmuir* **2006**, 22, 10457–10464.